Title	Quantum waveguide theory of serial stub structures
Author(s)	Jin, GJ; Wang, ZD; Hu, A; Jiang, SS
Citation	Journal Of Applied Physics, 1999, v. 85 n. 3, p. 1597-1608
Issued Date	1999
URL	http://hdl.handle.net/10722/42447
Rights	Creative Commons: Attribution 3.0 Hong Kong License

Quantum waveguide theory of serial stub structures

G. J. Jin
Department of Physics, The University of Hong Kong, Pokfulam Road, Hong Kong, People's Republic of China and Department of Physics and National Laboratory of Solid State Microstructures, Nanjing University, Nanjing 210093, People's Republic of China

Z. D. Wang[a)]
Department of Physics, The University of Hong Kong, Pokfulam Road, Hong Kong, People's Republic of China

A. Hu and S. S. Jiang
Department of Physics and National Laboratory of Solid State Microstructures, Nanjing University, Nanjing 210093, People's Republic of China

(Received 23 July 1998; accepted for publication 13 October 1998)

The electronic behaviors in quantum wires with serial stubs are studied. A general theory of quantum waveguide based on transfer matrix method is developed and is used to treat periodic stub structures, serial stub structures with a defect stub, and Fibonacci stub structures. A number of interesting physical properties in connection with electronic transmission, energy spectra, and charge density distributions in these structures, are found theoretically. In particular, we find that whether there are periodicity and symmetry in the transmission and energy spectra depends on the commensurability of the length parameters. If one length ratio is incommensurate, then the transmission and energy spectra do not exhibit periodicity and symmetry even for periodic stub structures. In particular, the quasiperiodic behaviors are shown in Fibonacci stub structures proposed by us whenever the length parameters are commensurate. The experimental relevance is also addressed briefly. © *1999 American Institute of Physics.* [S0021-8979(99)05002-1]

I. INTRODUCTION

Electronic behaviors in one-dimensional periodic, disordered and quasiperiodic structures are important subjects in condensed matter physics.[1,2] Historically, there have been many well-known models, such as the Kronig-Penney model, describing an electron in a one-dimensional periodic structure. In spite of the simplicity, these models display many main features of periodic structures, especially bands and gaps, so they have been introduced in the course of solid state physics. All electrons occupy the extended states in one-dimensional periodic structures.[3] Since there exists disorder, for example, impurities or defects, in otherwise periodic structures, localized modes may appear. Particularly, the scaling theory of localization indicates that any disorder will give rise to localized modes in one-dimensional systems.[4] It has been found theoretically that the one-dimensional quasiperiodicity of Fibonacci structures has substantial effects on energy spectra and eigenstates which are intermediate between periodic and disordered structures. The energy spectra are singular continuous and the eigenstates are critical.[5]

In recent years, there has been significant progress in one-dimensional physics, which has been not only a heuristic tool but also a real physical entity. On one hand, many polymer materials with long molecular chains can be regarded as one- or quasi-one dimensional;[6] on the other hand, many artificial structures, for example, quantum wires, have one-dimensional characteristics.[7,8] We are concerned with the latter which belongs to mesoscopic physics.[9–11] In a mesoscopic system, the essence is that an electron can transport coherently across the whole system with negligible inelastic scattering. As a result, a variety of interesting interference phenomena can be exhibited, such as the quantized conductance in the point contacts, persistent currents in metallic loops, universal conductance fluctuations, etc., which provide potential applications to the fabrication of new quantum interference devices.

With recent significant advancement in the fabrication technology of ultrasmall structures,[12] the molecular beam epitaxy together with electron-beam lithography can provide us with many mesoscopic metal or semiconductor structures. Furthermore, the scanning tunneling microscope has made it possible to fabricate atomic-scale structures. Using these techniques, one can make extremely high mobility quantum wires with narrow widths, in which only a few of the lowest subbands are occupied and the transport is approximately ballistic. The allowed modes in the quantum wires are then considered to be the waveguide modes. Since electronic transport in quantum wires with various geometric structures is not only a basic physical problem but also relevant to useful electronic devices, it has attracted considerable attention, in particular, the quantum waveguide theory has been used extensively.[13–17] For example, Sols *et al.* studied semiconductor stub structures that may exhibit transistor function.[13] The theoretical calculation showed that relatively small changes in the stub length can induce significant variation in the electron transmission across the structure. There

a)Electronic mail: zwang@hkucc.hku.hk

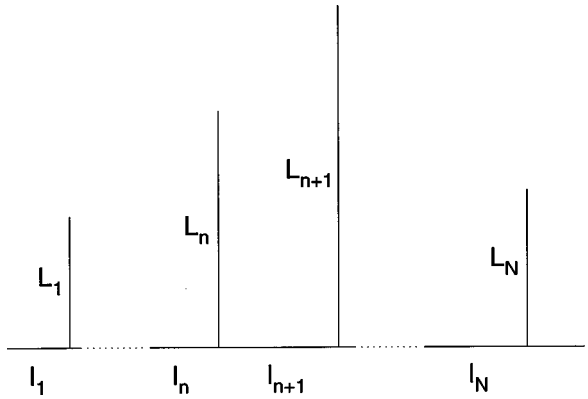

FIG. 1. A schematic serial stub structure. The lengths of the nth segment and nth stub are l_n and L_n, respectively.

have also been some experiments to successfully verify the waveguide characteristics of electron transport through a wide-narrow-wide structure by the splitting-gate technique.[18,19] In fact, more strikingly, many theoretical predictions in mesoscopic physics have now been (or will be in the near future) verified by experiments.

In this article, we systematically study electronic transport in quantum wires with serial stubs, in which disorder and interactions are assumed to be negligible. In Sec. II, using the transfer matrix method, we develop a general theory of quantum waveguide with serial stub structures. The theory is used to treat the periodic stub structures in Sec. III, the serial stub structures with a defect stub in Sec. IV, and Fibonacci stub structures in Sec. V. In Sec. VI, a brief summary and remarks are presented.

II. GENERAL THEORY

Recently, electronic transport of quantum waveguide structures has been addressed considerably.[13–15] Xia proposed a simple one-dimensional waveguide theory for quantum wires with one or two stubs.[16] Deo and Jayannavar extended it to multiple serial stub structures.[17] In this article, we consider a quantum wire attached with a series of stubs perpendicular to it as shown in Fig. 1. We label the wire segments with stubs one by one with positive integers n from left to right. In general, the lengths of the segments and stubs may vary along the wire. When the lateral cross section of the wire is sufficiently small and at sufficiently low temperatures, electrons can only occupy a few lowest transverse quantum states, and there are strong confinements in the two transverse directions, then only electronic motion in the longitudinal direction is of interest. The system considered is quasi-one-dimensional and retains quantum interference. It is assumed that no other scattering potentials are present except for the geometrical effect of the intersections of the stubs with the main wire, and only back scattering is the relevant scattering mechanism. So in any segment or stub, an electron is free particle-like. An electron with energy $\epsilon=\hbar^2k^2/2m$ (k is the wave vector but can also be used to represent the energy itself) injected from one side could pass through the structure ballistically, provided that the continuum conditions are satisfied. Also for simplicity, we use the Griffith boundary conditions below, which ensure the continuity of wave functions and the conservation of current density.

The electronic wave functions in the nth segment and nth stub are plane wave-like: $\psi_n(z)=A_n\exp(ikz)+B_n\times\exp(-ikz)$ and $\phi_n(z)=C_n\exp(ikz)+D_n\exp(-ikz)$, respectively. Hereafter, a local coordinate is chosen for each segment or stub, with its origin being located at the left-hand side of the segment or downside of the stub. In Fig. 1, if the upper end of each stub which can be controlled by external gate voltage is rigid, by applying the matching conditions of wave functions and their derivatives at the intersections, the electronic amplitudes in the $(n+1)$th segment can be obtained from the nth segment as

$$\begin{pmatrix} A_{n+1} \\ B_{n+1} \end{pmatrix} = T_{n+1,n}\begin{pmatrix} A_n \\ B_n \end{pmatrix}, \tag{1}$$

where $T_{n+1,n}$ is a 2×2 transfer matrix which can be written as

$$T_{n+1,n}=\begin{pmatrix} 1-\frac{i}{2}\cot(kL_n) & -\frac{i}{2}\cot(kL_n) \\ \frac{i}{2}\cot(kL_n) & 1+\frac{i}{2}\cot(kL_n) \end{pmatrix} \times\begin{pmatrix} e^{ikl_n} & 0 \\ 0 & e^{-ikl_n} \end{pmatrix}. \tag{2}$$

Since all the lengths l_n and L_n are combined with the wave vector k, we can take l_n and L_n as well as k to be dimensionless quantities in the following. By a transformation

$$\begin{pmatrix} A_n \\ B_n \end{pmatrix} = \begin{pmatrix} 1 & i \\ 1 & -i \end{pmatrix}\begin{pmatrix} \alpha_n \\ \beta_n \end{pmatrix}, \tag{3}$$

$T_{n+1,n}$ is transformed into $M_{n+1,n}$ for a new set of amplitudes (α_n,β_n), which satisfies the expression as

$$\begin{pmatrix} \alpha_{n+1} \\ \beta_{n+1} \end{pmatrix} = M_{n+1,n}\begin{pmatrix} \alpha_n \\ \beta_n \end{pmatrix}, \tag{4}$$

where

$$M_{n+1,n}=\begin{pmatrix} 1 & 0 \\ -\cot(kL_n) & 1 \end{pmatrix}\begin{pmatrix} \cos(kl_n) & -\sin(kl_n) \\ \sin(kl_n) & \cos(kl_n) \end{pmatrix}. \tag{5}$$

A specific merit of Eq. (5) is its form of real functions, which will give tremendous convenience for further analytic treatment. All of the transfer matrices $M_{n+1,n}$s$\in$SL(2,R), the set of all real 2×2 matrices with determinant one. If the lengths of all segments and stubs and the initial values of the amplitudes (α_1,β_1) are known, then all the amplitudes along the wire can be obtained recursively from

$$\begin{pmatrix} \alpha_{n+1} \\ \beta_{n+1} \end{pmatrix} = M(n)\begin{pmatrix} \alpha_1 \\ \beta_1 \end{pmatrix}, \tag{6}$$

where $M(n)=\Pi_{i=1}^{n}M_{i+1,i}$. In fact, when we treat electronic transport of the serial stub structure, the incident electron of the system is described by $\exp(ikz)$, and the reflection amplitude is R which can be obtained from the global transfer matrix, then $\alpha_1=(1+R)/2$, and $\beta_1=(1-R)/2i$. The system becomes deterministic.

For the wire with N serial stubs, after all of the transfer matrices $M(n)$s are obtained, many important physical quantities can be readily derived. As the global transfer matrix $M(N)=\Pi_{i=1}^{N}M_{i+1,i}$, the reflection amplitude is

$$R=-\frac{1}{2+|M(N)|^2}\{[M_{11}^2(N)-M_{12}^2(N)+M_{21}^2(N)-M_{22}^2(N)]-2i[M_{11}(N)M_{12}(N)+M_{21}(N)M_{22}(N)]\}, \tag{7}$$

and the transmission coefficient is

$$T_N=\frac{4}{2+|M(N)|^2}, \tag{8}$$

where $|M(N)|^2=\Sigma_{\mu,\nu}|M_{\mu,\nu}(N)|^2(\mu,\nu=1,2)$ is the sum of the squares of the four matrix elements. By using the periodic boundary condition of the finite serial stub structure, the energy spectra can also be obtained from

$$|\tfrac{1}{2}\,\mathrm{Tr}M(N)|\leqslant 1. \tag{9}$$

On the other hand, charge density distribution in the nth segment is determined by

$$|\psi_n(z)|^2=|A_n e^{ikz}+B_n e^{-ikz}|^2=2[|\alpha_n|^2+|\beta_n|^2+(|\alpha_n|^2-|\beta_n|^2)\cos(2kz)-(\alpha_n\beta_n^*+\alpha_n^*\beta_n)\sin(2kz)], \tag{10}$$

where

$$|\alpha_n|^2\pm|\beta_n|^2=\frac{1}{2+|M(N)|^2}\{[M_{11}^2(n)\pm M_{21}^2(n)][M_{12}^2(N)+M_{22}^2(N)]+[M_{12}^2(n)\pm M_{22}^2(n)][M_{11}^2(N)+M_{21}^2(N)]-[M_{11}(n)M_{12}(n)\pm M_{21}(n)M_{22}(n)][M_{11}(N)M_{12}(N)+M_{21}(N)M_{22}(N)]\} \tag{11}$$

and

$$\alpha_n\beta_n^*+\alpha_n^*\beta_n=\frac{2}{2+|M(N)|^2}\{M_{11}(n)M_{21}(n)[M_{12}^2(N)+M_{22}^2(N)]+M_{12}(n)M_{22}(n)[M_{11}^2(N)+M_{21}^2(N)]-[M_{12}(n)M_{21}(n)+M_{11}(n)M_{22}(n)][M_{11}(N)M_{12}(N)+M_{21}(N)M_{22}(N)]\}. \tag{12}$$

Equations (5) and (8)–(12) are some general results of quantum waveguide theory for serial stub structures, which will be used to treat periodic stub structures, serial stub structures with a defect stub, and Fibonacci stub structures in the next three sections.

III. PERIODIC STUB STRUCTURES

We would like to point out first that it is possible for us to consider some more complicated periodic stub structures with more than one segment and stub in each cell, but we here would rather discuss the simplest case in which there is only one type of building block, i.e., $l_n=l$ and $L_n=L$ for any n in Fig. 1. This is a very simple case where only one basic transfer matrix $M_{n+1,n}=M$ exists, and

$$M=\begin{pmatrix} m_{11} & m_{12}\\ m_{21} & m_{22}\end{pmatrix}=\begin{pmatrix} \cos(kl) & -\sin(kl)\\ \sin(kl)-\cos(kl)\cot(kL) & \cos(kl)+\sin(kl)\cot(kL)\end{pmatrix}. \tag{13}$$

As for $n=1,\ldots,N$, it is easy to show that

$$M(n)=M^n=\begin{pmatrix} m_{11}\mathscr{U}_{n-1}(x)-\mathscr{U}_{n-2}(x) & m_{12}\mathscr{U}_{n-1}(x)\\ m_{21}\mathscr{U}_{n-1}(x) & m_{22}\mathscr{U}_{n-1}(x)-\mathscr{U}_{n-2}(x)\end{pmatrix}, \tag{14}$$

where

$$x=\tfrac{1}{2}(m_{11}+m_{22})=\cos(kl)+\tfrac{1}{2}\sin(kl)\cot(kL) \tag{15}$$

and $\mathscr{U}_n(x)$ is a Chebyshev polynomial of the second kind[20,21] satisfying the second order differential equation as

$$(1-x^2)\mathscr{U}_n''(x)-3x\mathscr{U}_n'(x)+n(n+2)\mathscr{U}_n(x)=0. \tag{16}$$

The prime represents the derivative operator. For convenience, we consider the solutions of Eq. (16) to be in real form. Then for $|x|\leqslant 1$, we can take $x=\cos\theta$, and $\mathscr{U}_n(x)=\sin[(n+1)\theta]/\sin\theta$; but for $|x|\geqslant 1$, we define $|x|=\cosh\theta$, and $\mathscr{U}_n(x)=\sinh[(n+1)\theta]/\sinh\theta$ for $x>1$, and $(-1)^{n-1}\sinh[(n+1)\theta]/\sinh\theta$ for $x<-1$. There is a recursion relation

$$\mathscr{U}_n(x)=2x\mathscr{U}_{n-1}(x)-\mathscr{U}_{n-2}(x) \tag{17}$$

for any x.

Take $n=N$ in Eq. (14) and after some calculations, we can show

$$|M(N)|^2=2+F^2(N,k,l,L), \tag{18}$$

where

$$F(N,k,l,L)=\cot(kL)\mathscr{U}_{N-1}(x) \tag{19}$$

and the transmission coefficient is

$$T_N=\frac{4}{4+F^2(N,k,l,L)}. \tag{20}$$

This is a precise analytic expression which can be used to examine all results of periodic stub structures in Ref. 17. It is noted that Eq. (20) has a similar form for an electron passing through finite Dirac combs.[22] However, our approach is simple and independent. As shown by numerical calculations in Ref. 17, the transmission spectra have periodicity and symmetry for wave vectors k in some special length parameters. From Eqs. (19) and (20), we can discuss these problems more clearly and easily. In addition, we can also see from Eqs. (19) and (20) that there may exist some resonant transmission points ($T_N=1$) when eigenvalues k satisfying $F(N,k,l,L)=\cot(kL)\mathscr{U}_{N-1}(x)=0$ (on the other hand, any k satisfying $F(N,k,l,L)\rightarrow\pm\infty$ leads to a zero transmission). Resonant transmission can be obtained by requiring

$$\cos(kL)=0 \tag{21}$$

or

$$\sin(N\theta)=0, \quad \text{but } \sin\theta\neq 0. \tag{22}$$

The solutions of Eq. (21) are simply given by

$$kL=(2m+1)\pi/2, \tag{23}$$

where m is any non-negative integer. The solutions of Eq. (22) lead to

$$\cos(kl)+\frac{1}{2}\sin(kl)\cot(kL)=\cos\left(\frac{\gamma}{N}\pi\right), \tag{24}$$

where γ may take $1,\ldots,N-1,N+1,\ldots,2N-1$.

These resonant transmission points can be considered to be characteristics of periodicity and symmetry of transmission spectra. It will be clear at once that the periodicity and symmetry of the transmission spectra are closely related to the relative ratio of l and L. For convenience, in this section, we always take $L=1$. We note that there are two distinct cases: the commensurate case when l is a rational number and the incommensurate case when l is an irrational number. For the commensurate case, the periodicity and the symmetry always exist, which can be seen from the following two typical examples. (1) When $L=l=1$, Eq. (24) is written as $(3/2)\cos k=\cos(\gamma\pi/N)$. Because T_N is an even function of k in this example, the period of the transmission spectra is $\Delta k=\pi$ and the first period is $k\in(0,\pi]$, with its symmetric center located at $k=\pi/2$. For odd N, since there are $N-1$ eigenvalues of k satisfying Eq. (22) (corresponding to $\gamma=1,\ldots,N-1$), plus $k=\pi/2$ for Eq. (21), there are totally N resonant transmission points; for even N, there are also $N-1$ eigenvalues of k satisfying Eq. (22), but $\gamma=N/2$ gives $k=\pi/2$ overlapping with one of the solutions of Eq. (21), so there are totally $N-1$ resonant transmission points. (2) When $L=1$, $l=1/2$, then $[6\cos^2(k/2)-1]/4\cos(k/2)=\cos(\gamma\pi/N)$. The period of k for transmission spectrum is 2π, and the symmetric center of first period is at $k=\pi$. There are $2N-2$ values for $\gamma=1,\ldots,N-1,N+1,\ldots,2N-1$ to satisfy Eq. (22). For odd N, the resonant transmission points of k take $2N-2$ values, while for even N, plus additional $k=\pi/2$ and $3\pi/2$ satisfying Eq. (21) [but not satisfying Eq. (22)], there are $2N$ resonant transmission points. Figure 2(a) presents the numerical results of the first two periods for $N=6$. In Fig. 2(a), there are 12 resonant transmission points in the first period and the second period, respectively. Our method for discussing the periodicity and symmetry as well as for the calculation of the resonant transmission points can be readily used in other commensurate cases. Actually, in more general commensurate cases, $l=q/p$, p and q are integers which are relatively prime. Equation (15) is then $x=\cos(qk/p)+(1/2)\sin(qk/p)\cot k$. It can be seen that when $k\rightarrow p\pi+k$, then $x\rightarrow(-1)^q x$, the transmission coefficients are identical for both wave vectors, so the period of k is $\Delta k=p\pi$.

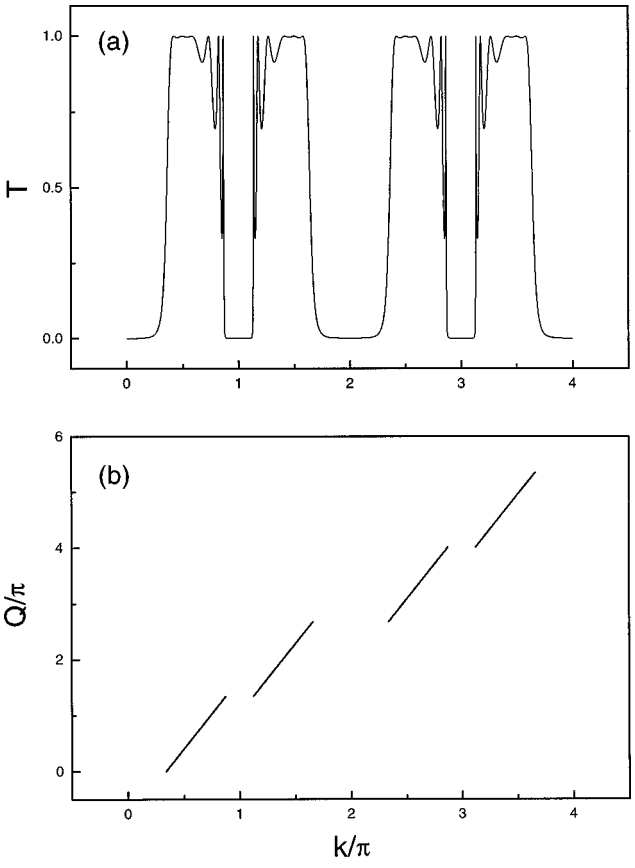

FIG. 2. The first two periods of the transmission spectrum and dispersion curve for a periodic stub structure with parameters $L=1$, $l=1/2$ and $N=6$. (a) Transmission coefficient T vs the incident wave vector k; (b) the wave vector of system Q vs k.

To the best of our knowledge, the incommensurate case has not been discussed in literature so far, but it is of interest. In this case, l is an irrational number. Then we cannot find any periodicity and symmetry for the transmission spectra as k varies, or to say, the period is infinite. This incommensurability for transmission spectra can be analyzed from Eqs. (15), (19) and (20), and one example is shown in Fig. 3(a) for which we take $l/L=(\sqrt{5}-1)/2$, the reciprocal of the well-known golden mean. Certainly, the resonant transmission points can still be determined from Eqs. (21) and (22).

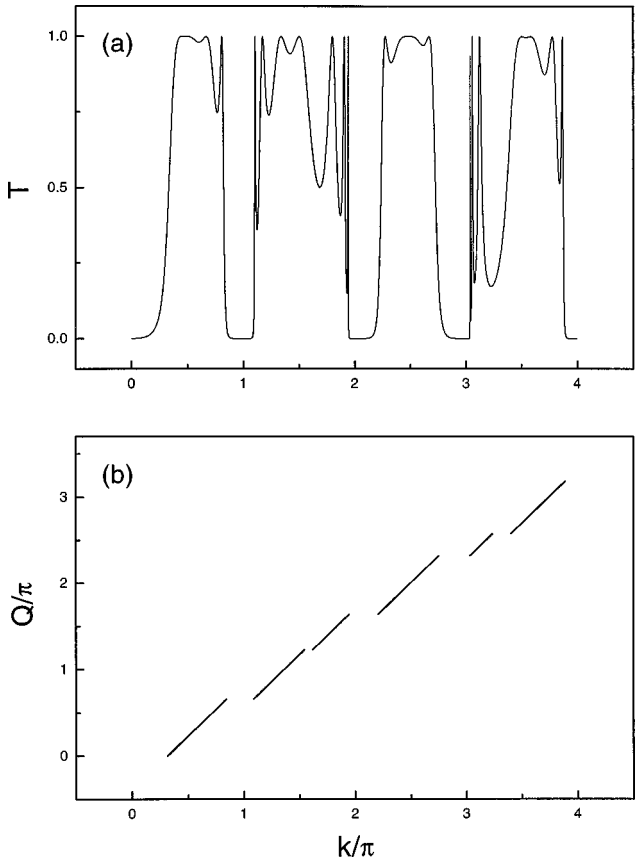

FIG. 3. A part of the transmission spectrum and dispersion curve for a periodic stub structure with parameters $L=1$, $l=(5^{1/2}-1)/2$, and $N=4$. (a) Transmission coefficient T vs the incident wave vector k; (b) the wave vector of system Q vs k.

Note that some of resonant transmission points determined from Eq. (23) are just as in the commensurate case, but others determined from Eq. (24) have no periodicity and symmetry. Nevertheless, we find from numerical calculations that there is a rule for the total number of resonant transmission points in the incommensurate case $l/L=(\sqrt{5}-1)/2$. For $k\in(0,2\pi]$, or $(2\pi,4\pi]$,..., the total number for resonant transmission points is invariant in each region once N is determined. For $N\geqslant 3$, when $N=$odd number, it is $3(N-1)$, but when $N=$even number, it is $3(N-2)$.

Strictly speaking, there are no rigorous transmission forbidden regions for finite serial stub structures. But as the number of stubs $\geqslant 4$, the high transmission regions are separated by the transmission valleys, which resemble forbidden regions. So transmission spectra can be compared with the energy band structures. Under the periodic approximation, by using Eqs. (9) and (14), we have

$$x\mathscr{U}_{N-1}(x)-\mathscr{U}_{N-2}(x)=\cos(QNl), \tag{25}$$

where Q is the wave vector of the system with a large ''unit cell'' of N segments.[23] Combined with Eq. (15), one can calculate the energy spectra of the periodic stub structures. The dispersion relations for commensurate and incommensurate cases are shown in Figs. 2(b) and 3(b). For clearness, we use the extended zone scheme for Q. Energy bands to high transmission region and energy gaps to transmission valleys are one to one correspondent.

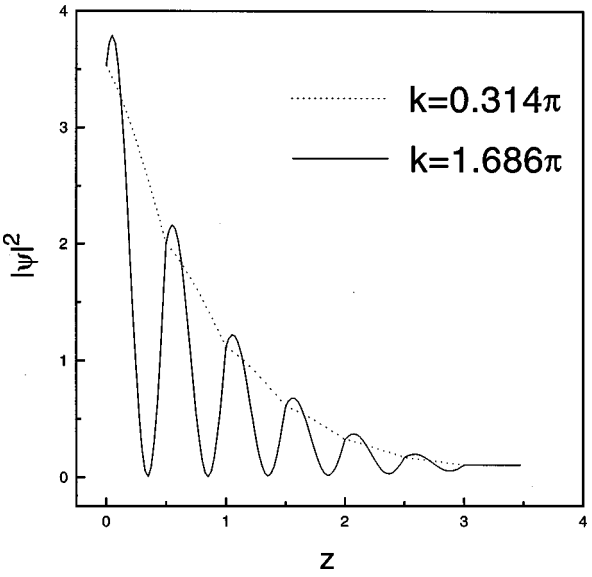

FIG. 4. The charge density distributions in a periodic stub structure for two symmetric wave vectors $k=0.314\pi$ and 1.686π in the first period of transmission spectrum with equal transmission coefficient $T=0.1025619$. The parameters are the same as those in Fig. 2.

There are close relations between transmission coefficients and charge density distributions of the system through transfer matrices. But it can be understood from Eqs. (10)–(12) that charge density distributions include more information than transmission coefficients. For a commensurate case $L=1$, $l=1/2$ and $N=6$, from the first two periods of the transmission and energy spectra shown in Fig. 2, we see that the period is $\Delta k=2\pi$ and the symmetric point of k is $2\pi-k$. By using Eq. (13), it is found that when $k\rightarrow 2\pi\pm k$ a couple of diagonal/off-diagonal matrix elements in Eq. (14) change their signs simultaneously (or not), thus Eqs. (11) and (12), which determine the envelopes of Eq. (10), remain invariant. However, $\cos(2kz)$ and $\sin(2kz)$ in Eq. (10) have no periodicity and symmetry for $k\rightarrow 2\pi\pm k$. Figure 4 shows the charge density distributions of two symmetric k values at the transmission band edges of the first period in Fig. 2(a) with transmission coefficient $T=0.1025619$. The charge density distribution decreases monotonically for $k=0.314\pi$, but decreases oscillatorily for $k=1.686\pi$. Both are localized modes exhibiting the characteristics of the edge states.

Figure 5 shows the charge density distributions for another commensurate example, $L=l=1$ and $N=11$, in which two wave vectors k chosen are located in the transmission interbands with resonant transmission coefficient $T=1$. We can see that they have the same envelopes for $k=0.3104799\pi$ and its periodic point $k=1.3104799\pi$.

For an incommensurate case, $L=1$ and $l=(\sqrt{5}-1)/2$, although the transmission and energy spectrum show incommensurate behavior as shown in Fig. 3, the charge density distributions do not exhibit such feature. In Fig. 6, we plot the results of a resonant transmission case with $N=100$ and $k=0.8199988\pi$, which clearly show a periodic distribution

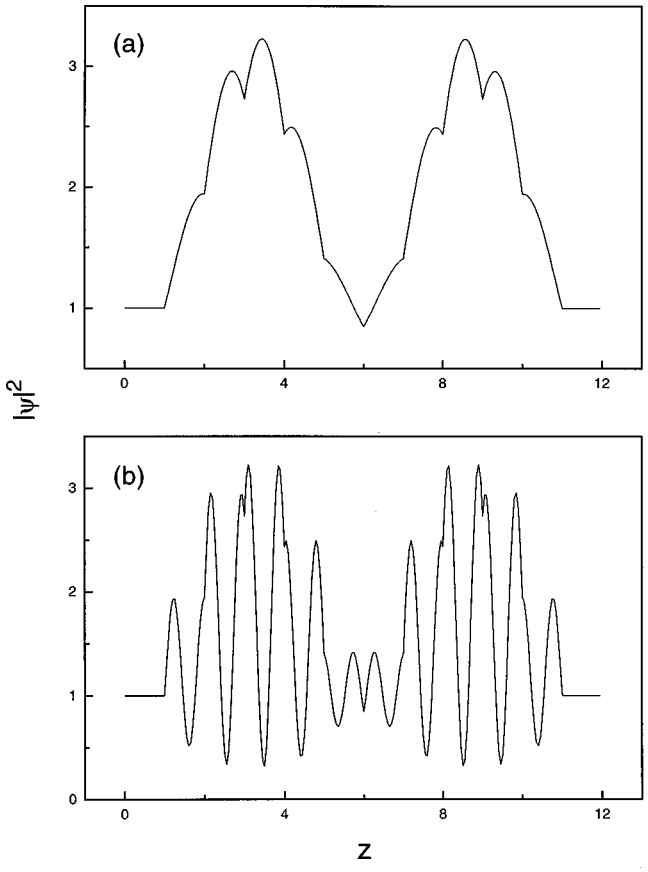

FIG. 5. The charge density distributions in a periodic stub structure for two periodic wave vectors in the first two periods with same resonant transmission coefficient $T=1$. The parameters are $L=l=1$, and $N=11$. (a) $k=0.3104799\pi$; (b) $k=1.3104799\pi$.

of the charge density. We wish to point out that in both commensurate and incommensurate cases for resonant transmission points corresponding to $k=\pi/2,3\pi/2,\ldots$, the charge density distributions are homogeneous, because an electron moves along the quantum wire as if there are no stubs, which can be directly seen from Eq. (13).

IV. SERIAL STUB STRUCTURES WITH A DEFECT STUB

As discussed by Deo and Jayannavar,[17] if there is a defect stub in an otherwise periodic stub structure, there may appear some positive energy bound states in the transmission

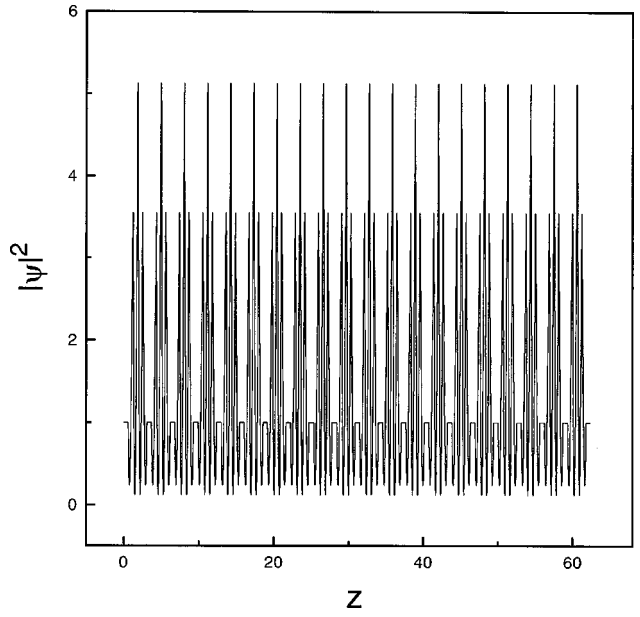

FIG. 6. The charge density distributions in a periodic stub structure for a resonant transmission wave vector $k=0.8199988\pi$. The parameters are $L=1$, $l=(5^{1/2}-1)/2$, and $N=100$.

spectra as shown in their Figs. 4 and 5. However, one of their conclusions that bound states disappear as the number of stubs increases is misleading. Actually, when we only improve the numerical calculation precision, we find that the bound states still exist with the same parameters as theirs in their Fig. 5, and the corresponding transmission coefficients are close to one. Notice that, in our treatment to be detailed below, unlike Ref. 17, we need not calculate the total transfer matrix from the numerical product of the individual transfer matrices and thus the numerical error will not be accumulated, leading to much smaller error, which appears to be crucial in some sensitive cases.

In a periodic semiconductor superlattice with a central artificial defect well, there is direct evidence of positive bound state, which is a spatially localized state formed by Bragg reflection.[24] Based on the similar physical origin, a defect stub in an otherwise periodic stub structure may induce spatially localized states by multiple reflections. We refer to the relevant wave vectors, i.e., energies, as isolated modes. If the length of the defect stub is L_d, then the transfer matrix corresponding to the defect stub reads

$$M_d=\begin{pmatrix} \cos(kl) & -\sin(kl) \\ \sin(kl)-\cos(kl)\cot(kL_d) & \cos(kl)+\sin(kl)\cot(kL_d) \end{pmatrix}. \tag{26}$$

For simplicity, we consider that the defect stub is located at the center of an otherwise periodic stub structure with S stubs arranged at each side of the defect stub and the total number of stubs being $N=2S+1$. The global transfer matrix is then

$$M(2S+1)=M^S M_d M^S. \tag{27}$$

After some tedious derivations, we obtain

$$|M(2S+1)|^2=2+F^2(2S+1,k,l,L,L_d), \tag{28}$$

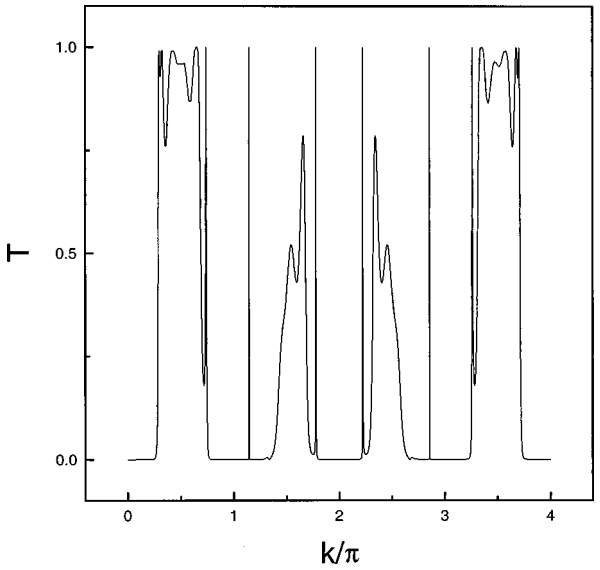

FIG. 7. The first period of the transmission spectrum for a serial stub structure with a defect stub. The parameters are $L=l=1$, $L_d=3/4$, $S=4$, and $N=2S+1=9$.

where

$$F(2S+1,k,l,L,L_d)=\cot(kL)[\mathscr{U}_S^2(x)-\mathscr{U}_{S-1}^2(x)] -[\cot(kL)-\cot(kL_d)][\mathscr{U}_S^2(x) -2\cos(kl)\mathscr{U}_S(x)\mathscr{U}_{S-1}(x) +\mathscr{U}_{S-1}^2(x)] \tag{29}$$

and x is still expressed in Eq. (15). The transmission coefficient is

$$T_{2S+1}=\frac{4}{4+F^2(2S+1,k,l,L,L_d)}. \tag{30}$$

As pointed out by Sols *et al.*, a small change in the stub length may induce dramatic changes in the transmission for a wide range of energy.[13] This is a remarkable result which may lead to useful device applications. Taking $L=l=1$, $L_d=0.75$, and $S=4$, from Eqs. (15), (29), and (30), we can determine that the period of transmission spectrum for k is 4π and the symmetric center of the first period is at $k=2\pi$. The transmission spectrum of the first period is shown in Fig. 7. We can see that a few resonant transmission peaks exist and some of them are thinner. How can one select the isolated modes? This question appears to be important, but is yet to be answered. Deo and Jayannavar[17] found only two isolated modes in the forbidden regions for the periodic stub structures if S is not too large. But it may not be reliable to depend on the limited numerical results mainly because of the restriction on the calculation precision of their method. We think it is constructive to address the problem as follows. In the absence of any defect stub, i.e., $L_d=L$ in Eq. (29), the high transmission regions forming bands correspond to $|x|\leqslant 1$; but when $L_d\neq L$, there may exist narrow transmission bands satisfying $|x|>1$. Furthermore, in each of the narrow transmission bands, there may exist a resonant transmission point, so we define the isolated modes as the solutions of $F(2S+1,k,l,L,L_d)=0$ with $|x|>1$. From this criterion, we can judge that there are six isolated modes in Fig. 7. They are $k=0.7390465\pi$, 1.1437939π, 1.7777596π, 2.2222404π, 2.8562061π, and 3.2609535π. These six isolated modes are symmetric about $k=2\pi$. Among them, the second and the fifth are two isolated modes already obtained in Ref. 17. Four other isolated modes are located at the edges of the original transmission bands, but they are really isolated modes as will be verified from the charge density distributions. When S increases, the positions of isolated modes will move a little. As $S\rightarrow\infty$, the condition of $F(2S+1,k,l,L,L_d)$ being finite leads to

$$\cot^2(kL_d)-2\cot(kL)\cot(kL_d)-4\cot(kl)\cot(kL)+4=0. \tag{31}$$

As $L=l=1$, $L_d=0.75$, six solutions of Eq. (31) are very close to the solutions for $S=4$. They are $k=0.7434217\pi$, 1.1438645π, 1.7781556π, 2.2218444π, 2.8561355π, and 3.2565783π.

As discussed before, in the periodic stub structures there are correspondences between the transmission spectra and the energy spectra. This is still true for the serial stub structures with a defect stub. From Eqs. (9) and (27), we have instead of Eq. (25)

$$x'\mathscr{U}_{2S}(x)-\mathscr{U}_{2S-1}(x)=\cos[Q(2S+1)l], \tag{32}$$

where

$$x'=\cot(kL)+\tfrac{1}{2}\sin(kl)\cot(kL_d). \tag{33}$$

Numerical calculation confirms that there are very narrow bands related to isolated modes in the transmission spectra, and they become narrower and narrower as S increases. This is consistent with the calculation on the density of states in Ref. 17.

The charge density distributions of serial stub structures with a defect stub can also be obtained by using Eqs. (10)–(12) with matrix elements given by Eqs. (13), (14), (26) and (27). Figure 8 shows the charge density distributions of two isolated modes $k=0.7411876\pi$ and 3.2588124π for $S=5$. It is noted that these two eigen-wave vectors are located between those for $S=4$ and $S=\infty$. The charge density distributions for these two symmetric modes separated from the original transmission bands have the same envelope, but there are more oscillations for larger k. It is seen from Fig. 8 that for these two isolated modes, as well as for four other isolated modes, charge density distributions exhibit the feature of localized states (bound states). The maximums of their envelopes are all at the center of the system. It can be expected that for larger S, the localization will be clearer, which has been confirmed in our numerical calculations up to $S=50$. After $S=10$, the charge density distribution of each isolated mode concentrates around the center of the structure with a very sharp peak. It can be roughly understood that the origin of the localized states is the condition for isolated modes, $|x|>1$, which leads to $\mathscr{U}_{n-1}(x)=\sinh(n\theta)/\sinh\theta$ or $(-1)^{n-1}\sinh(n\theta)/\sinh\theta$. For larger n, $\mathscr{U}_{n-1}\sim\exp(n\theta)$. The factor $\exp(n\theta)$ will enter into the Eqs.

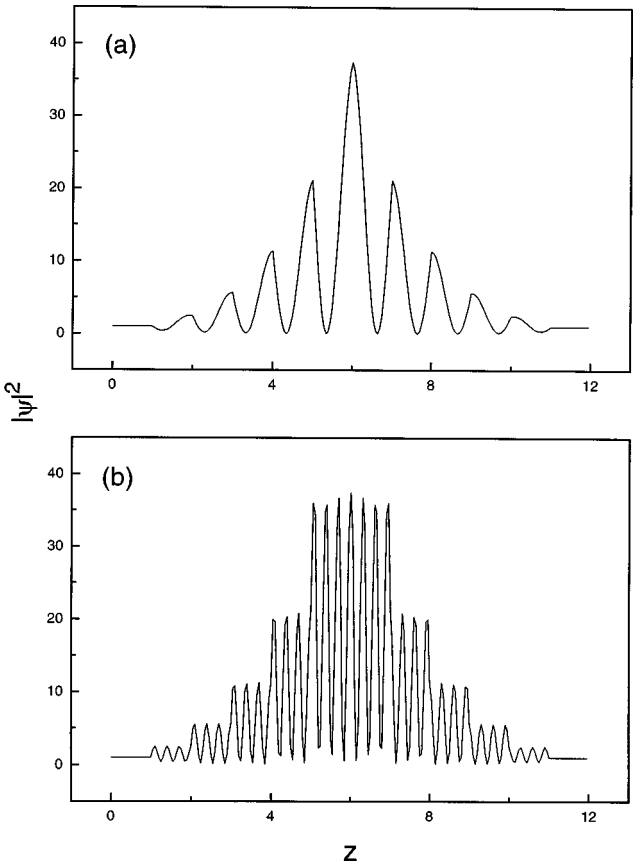

FIG. 8. The charge density distributions in a serial stub structure with a defect stub for two symmetric resonant transmission wave vectors in the first period of the transmission spectrum. The parameters are $L=l=1$, $L_d=3/4$, $S=5$, and $N=2S+1=11$. (a) $k=0.7411876\pi$; (b) $k=3.2588124\pi$.

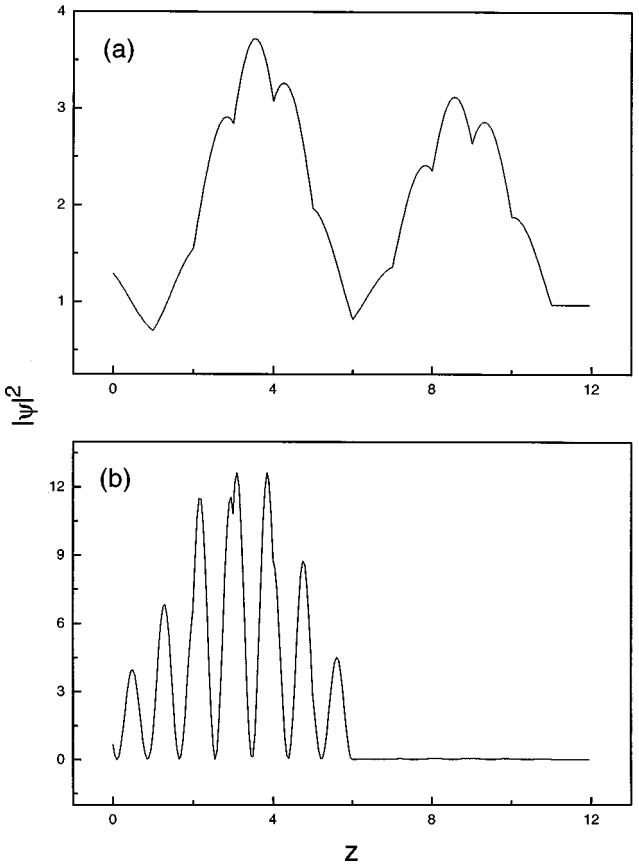

FIG. 9. The charge density distributions in a serial stub structure with a defect stub for two wave vectors the same as those in Fig. 5. The parameters are the same as those in Fig. 8. (a) $k=0.3104799\pi$, $T=0.9668976$; (b) $k=1.3104799\pi$, $T=0.0148286$.

(10)–(12), so the charge density distribution in the nth segment is related to the exponential factor $\exp(n\theta)$.

As has been seen that in the presence of a defect stub the transmission and energy spectra of an otherwise periodic stub structure change dramatically, especially when isolated modes corresponding to localized states appear. On the other hand, it is reasonable to believe that other states corresponding to the eigenvalues k satisfying $|x|\leqslant 1$ will also change a lot. Figure 9 shows the charge density distributions in the serial stub structure with a defect stub for the same two k values as in Fig. 5 for the periodic stub structure. The charge density distribution in Fig. 9(a) is somewhat similar to Fig. 5(a), but no symmetry about the center exists. The difference between Fig. 9(b) and Fig. 5(b) becomes even significant. Transmission coefficients $T=0.9668976$ for Fig. 9(a) and $T=0.0148286$ for Fig. 9(b).

Using the theoretical method introduced in this section, we can treat other serial stub structures with a defect stub, for examples, (1) $L=l=1$, $L_d=2$, $S=4$; and (2) $L=l=1$, $L_d=10$, $S=50$. From Eqs. (15), (29) and (30), the periods of the transmission spectra for both examples are $\Delta k=\pi$, so we only need to consider the first period $(0,\pi)$ which has the symmetry center at $k=\pi/2$. The solutions of $F(2S+1,k,l,L,L_d)=0$ with $|x|>1$ give out two isolated modes $k=0.2523298\pi$ and 0.7476702π for case (1); six isolated modes $k=0.0919845\pi$, 0.1795247π, 0.25π, 0.75π, 0.8204753π, and 0.9080155π for case (2). The numerical results of the charge density distributions for these isolated modes show that they are all localized states with maximum at the center of the structures.

We can also distinguish the commensurate and incommensurate behaviors in transmission spectra for serial stub structures with a defect stub. But now there are three parameters L, l, and L_d, so both l/L and L_d/L need to be considered. The situation will be more complicated. We have checked a simple example, $L=l=1$, $L_d=(\sqrt{5}-1)/2$. The transmission and energy spectra show no periodicity and symmetry at all, just like Fig. 3, but with different shapes. There are also some resonant transmission isolated modes. Their charge density distributions reflect the characteristics of localized states as well.

V. FIBONACCI STUB STRUCTURES

A Fibonacci stub structure is composed of two building units denoted by A and B. As shown in Fig. 1, unit A (B) is a wire segment of length $l_A(l_B)$ with a perpendicular stub of length $L_A(L_B)$ which can be varied by the external gate voltage. Using these two units, the Fibonacci stub structure is formed according to the rule $S_{j+1}=\{S_j,S_{j-1}\}$, with $S_1=A$ and $S_2=AB$. For example, $S_5=ABAABABA$. For simplic-

ity, we take the total segment number $N=F_j$, where j is the Fibonacci order and F_j is the Fibonacci number which satisfies $F_{j+1}=F_j+F_{j-1}$, with $F_1=F_0=1$. Corresponding to the two building units, there are two basic transfer matrices $M_{n+1,n}=M_A$ or M_B. From Eq. (5), the amplitude transformation of electron through unit A can be written as

$$M_A=\begin{pmatrix} \cos(kl_A) & -\sin(kl_A) \\ \sin(kl_A)-\cos(kl_A)\cot(kL_A) & \cos(kl_A)+\sin(kl_A)\cot(kL_A) \end{pmatrix}, \tag{34}$$

while for unit B, it is only needed to substitute $A\rightarrow B$ in the matrix expression of M_A to get M_B.

One can find a matrix map for Fibonacci structure as $M_{j+1}=M_{j-1}M_j$, with $M_0=M_B$ and $M_1=M_A$.[5] For a finite Fibonacci stub structure with $N=F_j$, the total transfer matrix of the system can be obtained by the recursion relation. The transmission coefficient of the N-unit system can be calculated from Eq. (8), and the energy spectrum from Eq. (9).

As there are four parameters of lengths for two real unimodular matrices M_A and M_B, the periodicity and symmetry of transmission spectra are determined by three length ratios, i.e., l_A/L_A, l_B/L_A, and L_B/L_A. When and only when l_A, l_B, L_A and L_B are all commensurate, the transmission and energy spectra have periodicity and symmetry for eigenvalues k. It is very interesting to note that in the incommensurate case the quasiperiodic behaviors for transmission and energy spectra are obscure. To examine the quasiperiodicity of the system more clearly, we consider only the commensurate cases below.

Typical results of electronic transmission through a Fibonacci stub structure are plotted in Fig. 10, where the parameters are $j=13$, $l_A=l_B=L_A=1$, $L_B=1/2$. Due to the periodicity and the symmetry of the transmission spectra, we need only consider the first half period $k\in(0,\pi]$ to show the quasiperiodic behaviors. From Fig. 10(a), we can see that transmission bands and gaps are tri-branching hierarchical and self-similar. Figure 10(b) is the enlargement of central region of Fig. 10(a). In fact, transmission bands and gaps correspond nearly to the electronic energy bands and gaps of the Fibonacci stub structure in the rational approximation.

To calculate the electronic energy spectra, we first get $M_{-1}=M_1M_0^{-1}$ from $M_0=M_B$ and $M_1=M_A$, then obtain

$$\begin{aligned} x_{-1}&=\cos[k(l_A-l_B)]+\tfrac{1}{2}\sin[k(l_A-l_B)][\cot(kL_A)\\ &\quad-\cot(kL_B)],\\ x_0&=\cos(kl_B)+\tfrac{1}{2}\sin(kl_B)\cot(kL_B),\\ x_1&=\cos(kl_A)+\tfrac{1}{2}\sin(kl_A)\cot(kL_A), \end{aligned} \tag{35}$$

where $x_j=(1/2)TrM_j$. For the present Fibonacci structure, the matrix map gives a trace map $x_{j+1}=2x_jx_{j-1}-x_{j-2}$, from which the energy spectra can be obtained in the rational approximation.[5] The formula used in the calculation is

$$x_j(k)=\cos(QF_jl). \tag{36}$$

All permitted k values are in the range $-1\leqslant\cos(QF_jl)\leqslant 1$. Figure 11 shows the energy spectrum with the same parameters of Fig. 10. The bands correspond to the transmission region, while the gaps forbidden region. The inset (a) of Fig. 11 is the enlargement of the central part which shows the self-similarity of the energy spectra, while the inset (b) of Fig. 11 gives the log-log plot of the total energy width W_j of j order Fibonacci stub structure with the Fibonacci number F_j. As is well known, the energy spectra of quasiperiodic structures form Cantor-like sets with Lebesque measure equal to zero. The self-similarity and scaling property of the energy spectra are characteristics of quasiperiodicity.[25,26]

Charge density distributions in Fibonacci structures are in general aperiodic and inhomogeneous, as the system is in the critical states. We here present two examples with parameters $l_A=l_B=L_A=1$, $L_B=1/2$, and $j=13$, as shown in Figs. 12(a) and 12(b). They, with different transmission probabilities, appear to display ''weak'' and ''strong'' statistical self-

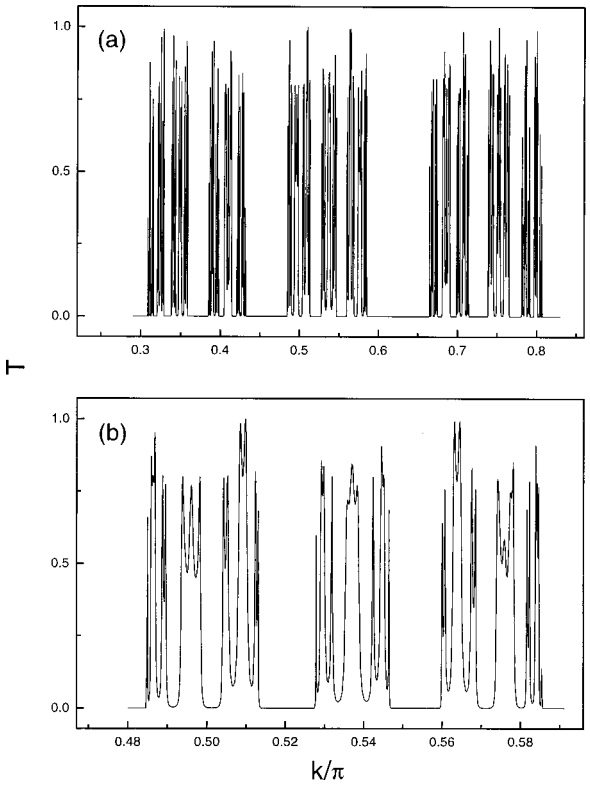

FIG. 10. The first half period of the transmission spectrum for a Fibonacci stub structure with parameters $L_A=l_A=l_B=1$, $L_B=1/2$, and $j=13$. (a) Transmission coefficient T vs the wave vector k; (b) the enlarged central part of (a).

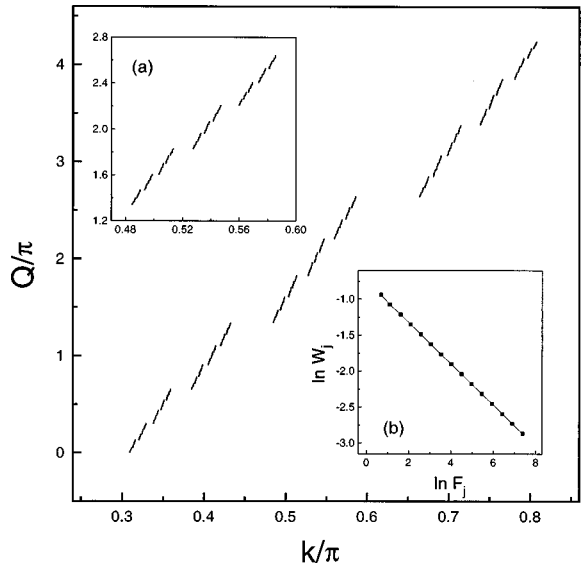

FIG. 11. The first half period of the energy spectrum of a Fibonacci stub structure with the same parameters as in Fig. 10. Inset (a) is the enlarged central part; inset (b) is the log-log plot of the total bandwidth W_j vs the Fibonacci number F_j for $j=2-16$.

similar behaviors. The transmission coefficients of Figs. 12(a) and 12(b) are $T=0.9997501$ and 0.1038452, respectively. From somewhat self-similar behavior and nearly resonant transmission shown in Fig. 12(a), we may ask if there

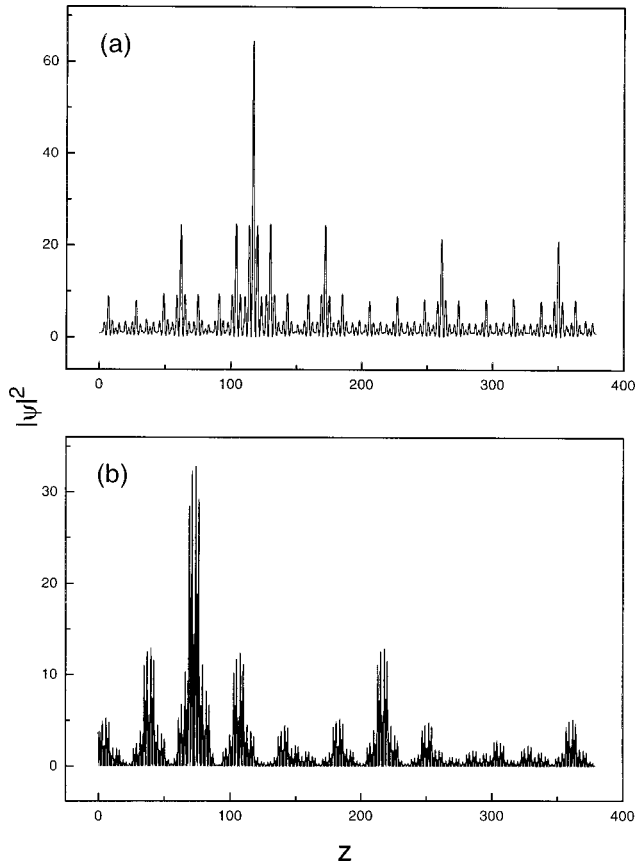

FIG. 12. The charge density distributions of a Fibonacci stub structure with the same parameters as those in Fig. 10. (a) $k=0.4094353\pi$, $T=0.9997501$; (b) $k=0.80625\pi$, $T=0.1038452$.

are eigenstates with both perfect resonant transmission and statistical self-similarity. In fact, from Eq. (8), perfect resonant transmission requires $|M(N)|^2=|M_j|^2=2$. According to the parametrization of the matrix elements,[27] the global transfer matrix M_j must be written in the form

$$M_j=\begin{pmatrix} \cos\varphi_j & \sin\varphi_j \\ -\sin\varphi_j & \cos\varphi_j \end{pmatrix}, \tag{37}$$

where φ_j is a phase factor determined by the parameters of the Fibonacci structure. However, since quasiperiodicity makes the energy spectra as well as transmission spectra to be singular continuous, we cannot expect that in self-similar states there are eigenvalues to fulfill this condition of perfect transmission.[28] Numerical calculations show that there is not any eigen k satisfying $|M_j|^2=2$.

An invariant $I=x_{j-1}^2+x_j^2+x_{j+1}^2-2x_{j-1}x_jx_{j+1}-1$ is usually chosen to characterize the quasiperiodicity of Fibonacci structures. As the expressions of x_{-1}, x_0, x_1 for Fibonacci stub structures have already been derived, it is easy to find a precise expression of I as

$$\begin{aligned} I=\tfrac{1}{4}\{&[\sin^2(kl_A)\cot(kL_B)-\sin^2(kl_B)\cot(kL_A)]^2 \\ &+[\sin(kl_A)\cos(kl_A)\cot(kL_B)-\sin(kl_B)\cos(kl_B) \\ &\times\cot(kL_A)]^2+\sin(kl_A)\sin(kl_B)\sin[k(l_A-l_B)] \\ &\times\cot(kL_A)\cot(kL_B)[\cot(kL_B)-\cot(kL_A)]\}. \end{aligned} \tag{38}$$

We here consider two simple cases. (1) $L_A=L_B=L$:

$$I=\tfrac{1}{4}\cot^2(kL)\sin^2[k(l_A-l_B)]. \tag{39}$$

In this expression, if $l_A=l_B$, then $I=0$, which corresponds to a periodic stub structure. If $l_A\neq l_B$, in general, $I\neq 0$ for most k eigenvalues and thus the quasiperiodicity plays a crucial role. (2) $l_A=l_B=l$:

$$I=\tfrac{1}{4}\sin^2(kl)[\cot(kL_A)-\cot(kL_B)]^2. \tag{40}$$

Periodicity appears when $L_A=L_B$. If we take $l_A=l_B=L_A=1$, $L_B=1/2$, then $I=0.25$; the quasiperiodic behaviors are clearly seen in Figs. 10, 11 and 12.

An impressive example to show the role of invariant I is in the central part of the transmission spectrum. The numerical results around $k=0.5372$ are shown in Figs. 13(a), 13(b), and 13(c) for $j=10,13,16$, respectively. It is interesting to note that they are very similar, but the widths of k in transmission regions are different. The width ratio $w_{10}/w_{13}=\alpha\approx 5.2$ for $j=10$ and 13 is almost the same as that w_{13}/w_{16} for $j=13$ and 16. In fact, $\alpha=[1+4(1+I)^2]^{1/2}+2(1+I)$ is just the scaling index of the renormalization group transformation of the six-cycle trace map.[5] Indeed $\alpha\approx 5.2$ if $I=0.25$. The fact that the fine structures of Fig. 13(a) are more similar to Fig. 13(c) than Fig. 13(b) implies that the six cycle is strict. We have also performed the numerical investigation to $j=9,12,15$, and $j=8,11,14$, and found that the six-cycle behavior is robust, although the patterns of transmission spectra are different from each other. Actually, this result for electronic transmission is analogous of electromagnetic waves in Fibonacci dielectric multilayers previously investigated theoretically and experimentally.[29] Although

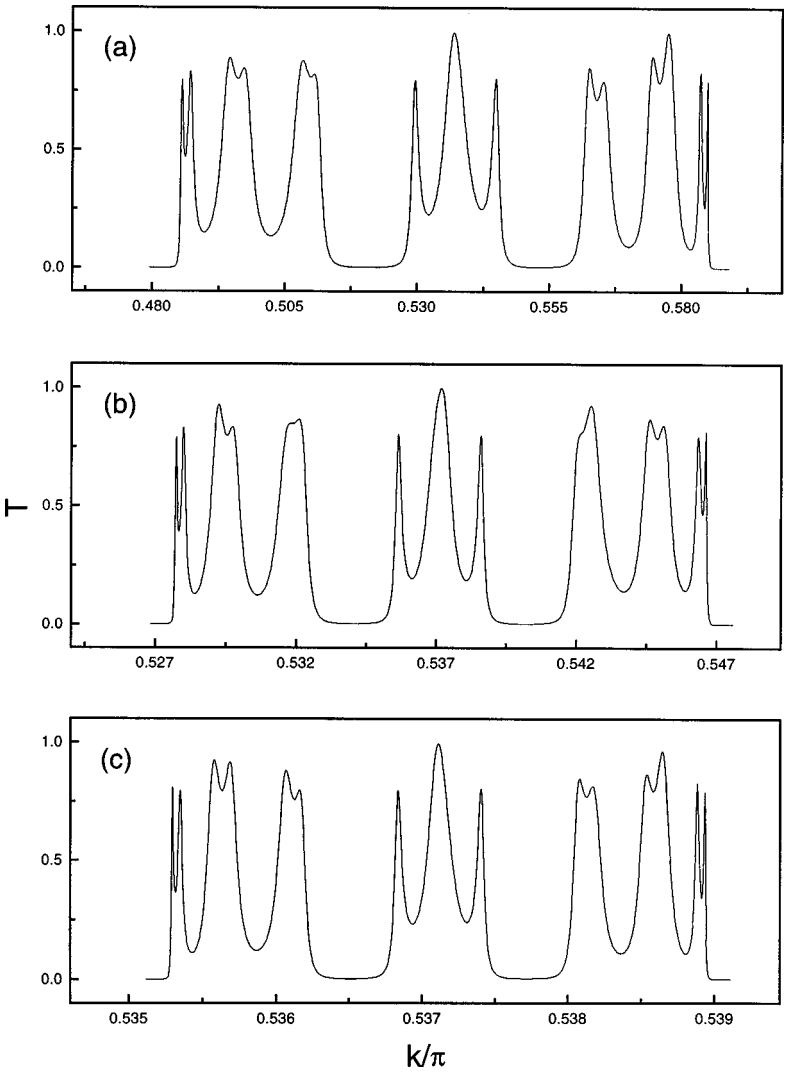

FIG. 13. The transmission spectra of a Fibonacci stub structure around $k=0.5372$, (a) $j=10$; (b) $j=13$; (c) $j=16$. The parameters are the same as those in Fig. 10.

significant theoretical efforts on electronic transport of Fibonacci structures have been made,[27,30] more experimental investigations are awaited, particularly those on the present mesoscopic structures proposed by us, which presents some challenge for experimentalists.[19]

VI. SUMMARY AND REMARKS

We have studied the electronic behaviors in quantum wires with serial stubs. A general theory of quantum waveguide based on the transfer matrix method has been developed and then is used to treat periodic stub structures, serial stub structures with a defect stub and Fibonacci stub structures. A number of interesting physical properties in connection with the electronic transmission, energy spectra and charge density distributions in these structures have been found theoretically. We have emphasized the important role of the relative ratios of lengths of segments and stubs, and found that whether there are periodicity and symmetry in the transmission and energy spectra depends on the commensurability of the length parameters. If there is one length ratio which is incommensurate, then the transmission and energy spectra have no periodicity and symmetry even for periodic stub structures. We have also proposed Fibonacci stub structures and have found that the length parameters chosen must be commensurate to exhibit the quasiperiodic behaviors. Because of this, except for a few incommensurate examples, we have paid much attention to the commensurate cases. The physical implications of the incommensurate cases are awaited to be further explored. The charge density distributions display the wave coherence in various serial stub structures. There are band edge localized states and extended states in the periodic stub structures, defect localized states as well as extended states in the serial stub structures with a defect stub, and critical states in the Fibonacci stub structures.

Although real quantum wires involve disorder and interactions, to capture quasi-one-dimensional feature and for simplicity, we have focused our attention to a single-channel free-electron model, which seems to be a reasonable approximation for the highly pure samples with significantly long mean free paths. In the network described by this model the scattering is solely determined by the geometric nature of the system, and the relevant quantum interference effects can be well understood. It is worth pointing out that transport properties of serial stub structures addressed here may be verified by experiments because, with the advances of nanofabrica-

tion technology, fabrication of various serial stub structures is feasible. For practical measurement, the transmission spectra discussed above are closely related to the conductance $G=(2e^2/h)T$.[31] Actually, at least two existing experiments appear to be relevant to our theoretical considerations. Kouwenhoven *et al.* have fabricated an artificial one-dimensional crystal with a corrugated channel in the two-dimensional electron gas of a GaAs-AlGaAs heterostructure by means of split-gate technique.[18] Its wide-narrow-wide structure is similar to the periodic stub structure discussed here and the subbands can be treated as independent current channels. The conductance measurement shows the bands and gaps which exhibit main features are somehow relevant to our results. Also, a Fibonacci lattice with corrugated 30 units was fabricated by Katsumoto *et al.* Their resistance measurement exhibited quasiperiodic behaviors.[19] We think that the proposed Fibonacci stub structure may be fabricated in a similar way, and thus the conductance measured may be compared with our results. On the other hand, the electromagnetic localized mode has been observed in optical waveguide of one-dimensional photonic crystal with a defect, and the defect, which behaved as a resonator or filter with relatively higher quality factor, is suggested.[32] It is therefore quite natural to believe that for the serial stub structure with a defect, a state located in the gap can also be detected and may play a useful role in device applications. Clearly, technological developments have led and will continue to lead to smaller and smaller scales of nanostructures which will miniaturize real electron devices further.

Our general theory can also be used to treat other aperiodic serial stub structures, such as Thue-Morse sequence, or even more disordered structures with defect stubs and defect segments. Different structures will lead to different transmission spectra which bring the benefits of band tailoring to device exploration.[7] It is also interesting, valuable, and challenging to take into account the electron-electron interactions in the serial stub structures. We hope the present work will stimulate more experimental and theoretical interests on similar mesoscopic structures.

ACKNOWLEDGMENTS

This work was supported by Hong Kong RGC Grant No. HKU262/95P and a CRCG grant at the HKU, the National Natural Science Foundation of China, the Provincial Natural Science Foundation of Jiangsu, and the Special Scientific Research Funds for Doctorate Candidates in Chinese Universities.

[1] *Highly Conducting One-Dimensional Solids*, edited by J. T. Devreese, R. P. Evrard, and V. E. van Doren (Plenum, New York, 1979).
[2] N. H. March and M. P. Tosi, Adv. Phys. **44**, 299 (1995).
[3] C. Kittel, *Introduction to Solid State Physics*, 7th ed. (Wiley, New York, 1996).
[4] E. Abrahams, P. W. Anderson, D. C. Licciardello, and T. V. Ramakrishnan, Phys. Rev. Lett. **42**, 673 (1979).
[5] M. Kohmoto, L. P. Kadanoff, and C. Tang, Phys. Rev. Lett. **50**, 1870 (1983); M. Kohmoto and Y. Oono, Phys. Lett. **102A**, 145 (1984); M. Kohmoto, B. Sutherland, and C. Tang, Phys. Rev. B **35**, 1020 (1987).
[6] A. Graja, *Low-Dimensional Organic Conductors* (World Scientific, Singapore, 1992).
[7] S. Datta and M. J. McLennan, Rep. Prog. Phys. **53**, 1003 (1990).
[8] G. Bastard, J. A. Brum, and R. Ferreira, in *Solid State Physics* (Academic, New York, 1991), Vol. 44, p. 229.
[9] *Quantum Coherence in Mesoscopic Systems*, edited by B. Kramer (Plenum, New York, 1991).
[10] *Mesoscopic Phenomenon in Solids*, edited by B. L. Altshuler, P. A. Lee, and R. A. Webb (North-Holland, Amsterdam, 1991).
[11] Y. Imry, *Introduction to Mesoscopic Physics* (Oxford University Press, New York, 1997).
[12] T. J. Thornton, Rep. Prog. Phys. **58**, 311 (1995).
[13] F. Sols, M. Macucci, U. Ravaioli, and K. Hess, Appl. Phys. Lett. **54**, 350 (1989); J. Appl. Phys. **66**, 3892 (1989).
[14] W. Porod, Z. Shao, and C. S. Lent, Appl. Phys. Lett. **61**, 1350 (1992); Z. Shao, W. Porod, and C. S. Lent, Phys. Rev. B **49**, 7453 (1994).
[15] J. R. Shi and B. Y. Gu, Phys. Rev. B **55**, 4703 (1997).
[16] J. B. Xia, Phys. Rev. B **45**, 3593 (1992).
[17] P. S. Deo and A. M. Jayannavar, Phys. Rev. B **50**, 11629 (1994).
[18] L. P. Kouwenhoven, F. W. J. Hekking, B. J. van Wees, C. J. P. M. Harmans, C. E. Timmering, and C. T. Foxon, Phys. Rev. Lett. **65**, 361 (1990).
[19] S. Katsumoto, N. Sano, and S. Kobayashi, Solid State Commun. **85**, 223 (1993).
[20] R. Courant and D. Hilbert, *Methods of Mathematical Physics I* (Interscience, New York, 1953).
[21] I. S. Gradshteyn and I. M. Ryzhik, *Table of Integrals, Series and Products* (Academic, New York, 1980).
[22] D. J. Griffiths and N. F. Taussig, Am. J. Phys. **60**, 883 (1992).
[23] S. Tamura and J. P. Wolfe, Phys. Rev. B **36**, 3491 (1987); S. Tamura and F. Nori, *ibid.* **40**, 9790 (1990).
[24] F. Capasso, C. Sirtori, J. Faist, D. L. Sivro, S. N. G. Chu, and A. Y. Cho, Nature (London) **358**, 565 (1992).
[25] P. Hawrylak and J. J. Quinn, Phys. Rev. Lett. **57**, 380 (1986).
[26] G. J. Jin, Z. D. Wang, A. Hu, and S. S. Jiang, J. Phys.: Condens. Matter **8**, 10285 (1996); Phys. Rev. B **55**, 9302 (1997); J. Phys. Soc. Jpn. **67**, 49 (1998).
[27] M. Kohmoto, Phys. Rev. B **34**, 5043 (1986); B. Sutherland and M. Kohmoto, *ibid.* **36**, 5877 (1987).
[28] G. J. Jin and Z. D. Wang, Phys. Rev. Lett. **79**, 5298 (1997).
[29] M. Kohmoto, B. Sutherland, and K. Iguchi, Phys. Rev. Lett. **58**, 2435 (1987); W. Gellermann, M. Kohmoto, B. Sutherland, and P. C. Taylor, *ibid.* **72**, 633 (1994).
[30] P. Hu and C. S. Ting, Phys. Rev. B **34**, 8331 (1986).
[31] R. Landauer, Z. Phys. B **68**, 217 (1987).
[32] J. S. Foresi, P. R. Villeneuve, J. Ferrera, E. R. Thoen, G. Steinmeyer, S. Fan, J. D. Joannopoulos, L. C. Kimerling, H. I. Smith, and E. P. Ippen, Nature (London) **390**, 143 (1997).